



Article

A Novel Carbon-Assisted Chemical Vapor Deposition Growth of Large-Area Uniform Monolayer MoS₂ and WS₂

Jeonghwan Bae¹ and Youngdong Yoo^{2,*} ¹ Department of Energy Systems Research, Ajou University, Suwon 16499, Korea; qowjdghks123@naver.com² Department of Chemistry, Ajou University, Suwon 16499, Korea

* Correspondence: yyoo@ajou.ac.kr

Abstract: Monolayer MoS₂ can be used for various applications such as flexible optoelectronics and electronics due to its exceptional optical and electronic properties. For these applications, large-area synthesis of high-quality monolayer MoS₂ is highly desirable. However, the conventional chemical vapor deposition (CVD) method using MoO₃ and S powder has shown limitations in synthesizing high-quality monolayer MoS₂ over a large area on a substrate. In this study, we present a novel carbon cloth-assisted CVD method for large-area uniform synthesis of high-quality monolayer MoS₂. While the conventional CVD method produces thick MoS₂ films in the center of the substrate and forms MoS₂ monolayers at the edge of the thick MoS₂ films, our carbon cloth-assisted CVD method uniformly grows high-quality monolayer MoS₂ in the center of the substrate. The as-synthesized monolayer MoS₂ was characterized in detail by Raman/photoluminescence spectroscopy, atomic force microscopy, and transmission electron microscopy. We reveal the growth process of monolayer MoS₂ initiated from MoS₂ seeds by synthesizing monolayer MoS₂ with varying reaction times. In addition, we show that the CVD method employing carbon powder also produces uniform monolayer MoS₂ without forming thick MoS₂ films in the center of the substrate. This confirms that the large-area growth of monolayer MoS₂ using the carbon cloth-assisted CVD method is mainly due to reducing properties of the carbon material, rather than the effect of covering the carbon cloth. Furthermore, we demonstrate that our carbon cloth-assisted CVD method is generally applicable to large-area uniform synthesis of other monolayer transition metal dichalcogenides, including monolayer WS₂.

Keywords: carbon-assisted CVD; growth mechanism; monolayer; MoS₂; WS₂



Citation: Bae, J.; Yoo, Y. A Novel Carbon-Assisted Chemical Vapor Deposition Growth of Large-Area Uniform Monolayer MoS₂ and WS₂. *Nanomaterials* **2021**, *11*, 2423. <https://doi.org/10.3390/nano11092423>

Academic Editor: Antonino Gulino

Received: 17 August 2021

Accepted: 14 September 2021

Published: 17 September 2021

Publisher's Note: MDPI stays neutral with regard to jurisdictional claims in published maps and institutional affiliations.



Copyright: © 2021 by the authors. Licensee MDPI, Basel, Switzerland. This article is an open access article distributed under the terms and conditions of the Creative Commons Attribution (CC BY) license (<https://creativecommons.org/licenses/by/4.0/>).

1. Introduction

Two-dimensional (2D) materials have attracted much attention due to their novel physical and chemical properties [1–5]. Graphene, the most studied 2D material, is thin, flexible, remarkably strong, and has exceptionally high electron mobility and thermal conductivity, allowing for a wide range of novel applications [1,2,6]. However, graphene has a zero bandgap, which results in very low on-off ratios in its applications of electronic devices such as transistors [4,5,7]. On the other hand, unlike graphene, transition metal dichalcogenides (TMDCs) have been intensively studied as new 2D layered materials because they have a sizable bandgap and interesting electronic and optical properties [3–5,7]. MoS₂, a family of TMDCs, has been used as a building block for 2D field-effect transistors due to its high carrier mobility and excellent on-off ratios [8–10]. In addition, due to its exceptional physicochemical properties, 2D MoS₂ has been extensively used for novel 2D electronics, flexible optoelectronics, and efficient catalysis [11–15]. When MoS₂ is thinned down to a monolayer, its electronic structure and physical symmetries are radically altered, resulting in new physical behavior such as indirect to direct bandgap transitions [16–18]. In addition, monolayer MoS₂ exhibits strong light–matter interactions due to its planar exciton confinement effect [16,19,20]. To increase the potential use of monolayer MoS₂ in

various applications, it is highly desirable to develop methods for preparing monolayer MoS₂ [8,10,11,15,21,22]. The most well-known mechanical exfoliation method is suitable for producing high-quality single crystalline MoS₂ flakes, but it cannot control the number of layers of the flakes and is unscalable for mass production [23–26]. In contrast, the chemical vapor deposition (CVD) method can control the number of MoS₂ layers and enables wafer-scale synthesis [27–29]. However, the conventional CVD method using MoO₃ and S powder has a problem in that thick MoS₂ films are formed in the center of the substrate and only MoS₂ monolayers are generated at the edge of the thick MoS₂ films [30–34].

This problem is related to the growth mechanism of MoS₂ in the conventional CVD method. The growth of MoS₂ is mainly achieved by the reaction of S with suboxide MoO_{3-x} species produced from MoO₃ powder [35–37]. MoO_{3-x} is highly volatile and improves the reaction kinetics for the formation of monolayer MoS₂ [35,37]. Monolayer MoS₂ can be effectively formed when the degree of MoO_{3-x} formation is sufficiently high, whereas thick MoS₂ films are generated when the degree of MoO_{3-x} formation is low. Therefore, keeping the degree of MoO_{3-x} formation high in the reaction process is a key condition for large-area uniform growth of high-quality monolayer MoS₂ without forming thick MoS₂ films. To achieve the large-area growth of monolayer MoS₂, various methods have been reported, including confined-space CVD, reverse-flow chemical vapor epitaxy, inorganic vapor CVD, and metal organic CVD, etc. [38–44].

In this study, we report a novel carbon cloth-assisted CVD method that uniformly produces high-quality monolayer MoS₂ over a large area on a substrate without forming thick MoS₂ films. As-synthesized monolayer MoS₂ was characterized in detail by Raman/photoluminescence (PL) spectroscopy, atomic force microscopy (AFM), and transmission electron microscopy (TEM). We reveal the detailed growth process of monolayer MoS₂ initiated from MoS₂ seeds by conducting a series of experiments with varying reaction times. In addition, we show that the CVD method employing carbon powder instead of carbon cloth also enables large-area growth of monolayer MoS₂, confirming the large-area growth of monolayer MoS₂ by the carbon cloth-assisted CVD method is mainly due to reducing properties of the carbon material, rather than the effect of covering the carbon cloth. Furthermore, we confirm that the carbon cloth-assisted CVD method can be used for the synthesis of other monolayer TMDCs such as monolayer WS₂.

2. Materials and Methods

2.1. Conventional CVD Method for MoS₂ and WS₂ Synthesis

MoS₂ was synthesized by a CVD method using a two-zone horizontal hot-wall tube furnace equipped with a mass flow controller and a vacuum pump (Edwards Vacuum, west Sussex, United Kingdom). The synthetic scheme is illustrated in Figure 1a. In a 1-inch diameter quartz tube, S powder (0.1 g, Sigma–Aldrich, St. Louis, MO, USA, 99.999%) in an alumina boat was placed upstream, and MoO₃ powder (0.03 g, Sigma–Aldrich, 99.5%) in an alumina boat was put downstream. The growth promoter solution that was prepared by supersaturating NaCl in ethanol was dropped on a clean 300-nm SiO₂/Si substrate and dried. NaCl serves as a promoter for the growth of MoS₂ [45]. Na⁺ in NaCl can react with MoO_{3-x} to form eutectic intermediates possessing a low melting point, promoting the growth of monolayer MoS₂. The 300-nm SiO₂/Si substrate was placed face down on the alumina boat containing MoO₃ powder. We used a vacuum pump to lower the pressure of the quartz tube to 5-mTorr or less to remove air in the quartz tube before the reaction. After turning off the vacuum pump, Ar gas (ultra-high purity, 99.999%, Dong-A Gases, Seoul, Korea) flowed at a rate of 100 sccm until reaching atmospheric pressure. After the pressure reached the atmospheric pressure, Ar gas flowed at a rate of 10 sccm. The temperatures of S and MoO₃ powder were independently controlled in two separate heating zones. The MoO₃ powder was heated to 740 °C for 15 min at a rate of ≈47.6 °C min⁻¹ and maintained at 740 °C for 20 min. The S powder was heated to 210 °C for 19 min at a rate of ≈9.7 °C min⁻¹ and maintained at 210 °C for 16 min. After the end of the reactions, the furnace lid was opened to cool the furnace rapidly to room temperature.

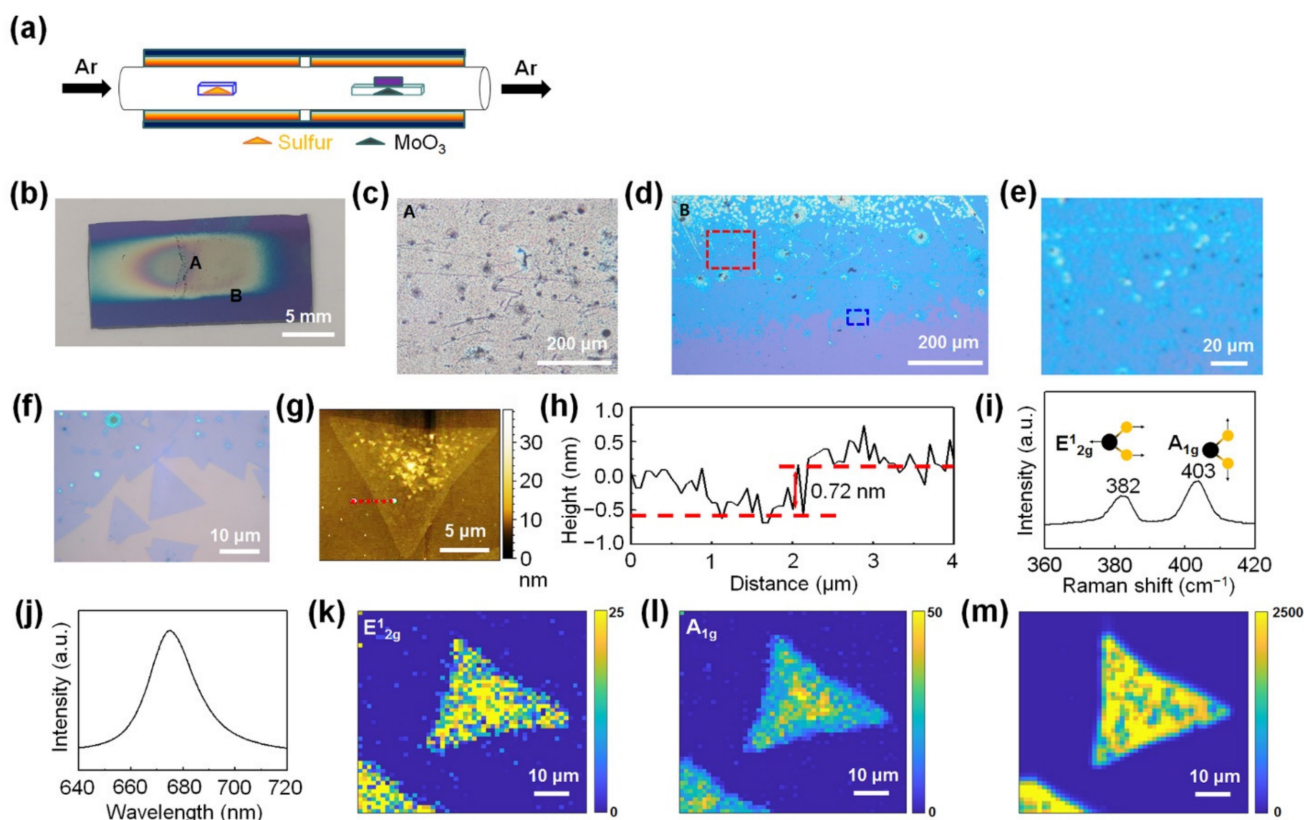


Figure 1. Conventional chemical vapor deposition (CVD) growth of MoS₂. (a) Schematic illustration of the experimental setup for the conventional CVD growth of MoS₂. (b) Optical image of the MoS₂ synthesized on an SiO₂/Si substrate using the conventional CVD method. (c) Magnified optical image of the region A in (b). (d) Magnified optical image of the region B in (b). (e) Magnified optical image of the dotted red rectangle in (d). (f) Magnified image of the dotted blue rectangle in (d). (g) Atomic force microscopy (AFM) height image of monolayer MoS₂ synthesized using the conventional CVD method. (h) Height line profiles along the dotted red line in (g). (i) Raman and (j) photoluminescence (PL) spectra of monolayer MoS₂. (k,l) Raman maps of the E_{2g} mode and A_{1g} mode of MoS₂, respectively. (m) PL map of monolayer MoS₂.

For the synthesis of monolayer WS₂, S powder (0.3 g, Sigma–Aldrich, 99.999%) and WO₃ powder (0.05 g, Sigma–Aldrich, 99.9%) were used as precursors. The c-cut sapphire substrate was placed face down on an alumina boat containing WO₃ powder. After the quartz tube was evacuated to 5-mTorr or less, Ar and H₂ gases flowed at a rate of 140 sccm and 20 sccm, respectively, and the chamber pressure was maintained at ≈1.6 Torr. The WO₃ powder was heated to 950 °C for 30 min at a rate of ≈30.8 °C/min and kept at 950 °C for 20 min. The S powder was heated to 210 °C for 32 min at a rate of ≈5.8 °C min^{−1} and maintained at 210 °C for 18 min.

2.2. Carbon Cloth-Assisted CVD Method for Monolayer MoS₂ and WS₂ Synthesis

The synthesis conditions of the carbon cloth-assisted CVD method are the same as those of the conventional CVD method described above, except that carbon cloth is placed on top of MoO₃ and WO₃ powder in an alumina boat for the synthesis of monolayer MoS₂ and WS₂, respectively.

2.3. Carbon Powder-Assisted CVD Method for Monolayer MoS₂ Synthesis

The synthesis conditions of the carbon powder-assisted CVD method are the same as those of the conventional CVD synthesis method described above, except that activated carbon powder is mixed with MoO₃ powder. The mixing ratios of MoO₃ powder to activated carbon powder used in each experiment were 1:1, 1:2, 1:3, 1:4, 1:5, and 1:10, respectively.

2.4. Characterization

Raman spectra and maps were obtained using a 532-nm laser with 100 μ W focused through a 100 \times objective at room temperature. Scanning electron microscopy (SEM) images and energy-dispersive X-ray spectroscopy (EDS) data were taken at 5 kV using a JSM-7900F (JEOL) microscope operating from 1 to 15 kV (JEOL Ltd., Tokyo, Japan). AFM measurement was performed in noncontact mode on an Anton–Paar Tosca 400 AFM instrument (Anton Paar, Sumida, Austria). TEM measurements were performed using a JEM-2100F microscope (JEOL Ltd., Tokyo, Japan).

3. Results and Discussion

3.1. Thick MoS₂ Films and Monolayer MoS₂ Synthesized Using the Conventional CVD Method

Figure 1a shows a schematic illustration of the experimental setup for the conventional CVD method in which solid powders (MoO₃ and S powder) are used as precursors for MoS₂ synthesis. Figure 1b shows an optical image of MoS₂ synthesized on a 300-nm SiO₂/Si substrate using the conventional CVD method. Figure 1c is a magnified optical image of region A in Figure 1b, showing the MoS₂ grown in the form of a thick film in the center of the substrate. Figure 1d is a magnified optical image of region B in Figure 1b, showing the edge region of the thick MoS₂ films. Figure 1e,f show magnified optical images of the dotted red rectangle and dotted blue rectangle in Figure 1d, respectively, confirming the partial formation of monolayer MoS₂ at the edge of the thick MoS₂ film. Additional data on the optical characterization of the MoS₂ grown using the conventional CVD method are shown in Supplementary Materials Figure S1. The growth of such thick MoS₂ films and partial formation of monolayer MoS₂ have been commonly observed in MoS₂ growth by the conventional CVD method using MoO₃ and S powder as precursors [30–34]. An AFM height image of monolayer MoS₂ shows small particles grown nonuniformly on the surface of monolayer MoS₂ (Figure 1g). The line profile obtained along the dotted red line in Figure 1g shows that the thickness of the synthesized monolayer MoS₂ is \sim 0.72 nm, which is consistent with the reported thickness of monolayer MoS₂ (Figure 1h) [19,46].

Raman and photoluminescence (PL) analyses were performed on the as-synthesized monolayer MoS₂. The Raman spectrum of monolayer MoS₂ shows that the frequency difference between the E_{2g}¹ mode located at 382 cm^{−1} and the A_{1g} mode located at 403 cm^{−1} was approximately 21 cm^{−1} (Figure 1i), which is consistent with that of the reported monolayer MoS₂ [31]. Due to the direct bandgap of monolayer MoS₂, the PL spectrum of MoS₂ shows a strong A exciton peak at 1.84 eV (Figure 1j) [19,47]. Raman and PL maps show that monolayer MoS₂ exhibited nonuniform Raman and PL peak intensities, confirming that monolayer MoS₂ had nonuniform optical and electronic properties (Figure 1k–m). Even when H₂ was used as a carrier gas with Ar for the MoS₂ synthesis, thick MoS₂ films were formed in the center of the substrate and some flakes of monolayer MoS₂ were partially formed at the edge of the thick films (Figure S2).

3.2. Monolayer MoS₂ Synthesized Using Carbon Cloth-Assisted CVD Method

Figure 2a shows a schematic illustration of the carbon cloth-assisted CVD growth of monolayer MoS₂. The experimental conditions were the same as those of the conventional CVD synthesis growth, except that the MoO₃ powder contained in the alumina boat was covered with carbon cloth. Unlike the conventional CVD method, this carbon cloth-assisted CVD method enables the growth of monolayer MoS₂ without forming thick films in the center of the substrate. Figure 2b is an optical image showing MoS₂ grown on a 300-nm SiO₂/Si substrate by the carbon cloth-assisted CVD method, confirming that there were no thick films in the center of the substrate. Figure 2c–e show the low-magnification and high-magnification optical images for regions A, B, and C in Figure 2b, respectively, confirming that monolayer MoS₂ grew relatively uniformly throughout the substrate without forming thick MoS₂ films in the center of the substrate. Additional data on the optical characterization of the MoS₂ grown using the carbon-assisted CVD method are shown in Figures S3 and S4. In addition, we observed that the size of the monolayer MoS₂

decreased when we moved from region A to region C in Figure 2b. The change in the size of the monolayer MoS₂ can be explained as follows; on regions A and B located upstream, a sufficient amount of S vapor reacts with MoO_{3-x} to form large monolayer MoS₂, whereas on region C located downstream, the amount of S vapor reaching region C is relatively small, resulting in relatively limited reactions with S vapor and MoO_{3-x}.

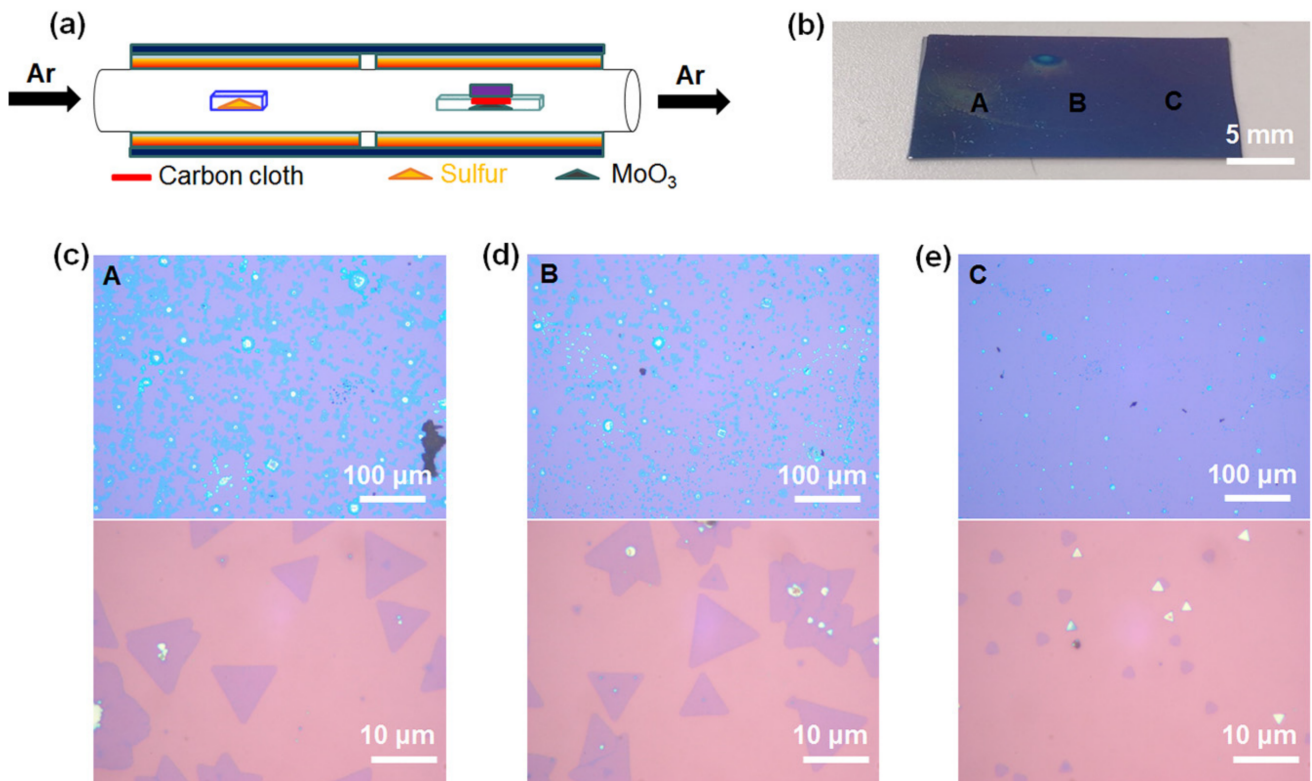


Figure 2. Carbon cloth-assisted CVD growth of monolayer MoS₂. (a) Schematic illustration of the experimental setup for carbon cloth-assisted CVD growth of monolayer MoS₂. (b) Optical image of monolayer MoS₂ grown on an SiO₂/Si substrate. Low-magnification and high-magnification optical images of (c) region A, (d) region B, and (e) region C in (b).

To investigate the mechanisms of the carbon cloth-assisted CVD growth of monolayer MoS₂, materials formed on carbon cloth during the growth were analyzed. Figure 3a,b show low-magnification and high-magnification SEM images of carbon cloth obtained after the carbon cloth-assisted CVD growth, respectively, confirming that the surface of the carbon cloth was entirely covered with nanoplates with a size of two to three microns. Raman analysis confirms that these nanoplates consisted of MoS₂ and MoO₂ (Figure 3c) [48]. In addition, EDS analysis shows that the nanoplates were composed of Mo, S, and O, and the proportion of O was very large compared to the proportion of S (Figure 3d), which confirms that the nanoplates were mostly composed of MoO₂ and were partially composed of MoS₂. MoO₂ is a byproduct that is frequently formed in the conventional CVD growth of MoS₂ using MoO₃ and S powder as precursors. MoO₂ is nonvolatile and has a high melting point, so it remains once it is formed on the substrate. One of the important roles of carbon cloth in carbon cloth-assisted CVD growth is to prevent MoO₂ from forming on the SiO₂/Si substrate by allowing MoO₂ to form on the carbon cloth (Figure S5). Another role of carbon cloth is to improve the reaction kinetics for MoS₂ growth by facilitating the formation of suboxide MoO_{3-x} species formed from MoO₃, as carbon acts as a reducing agent.

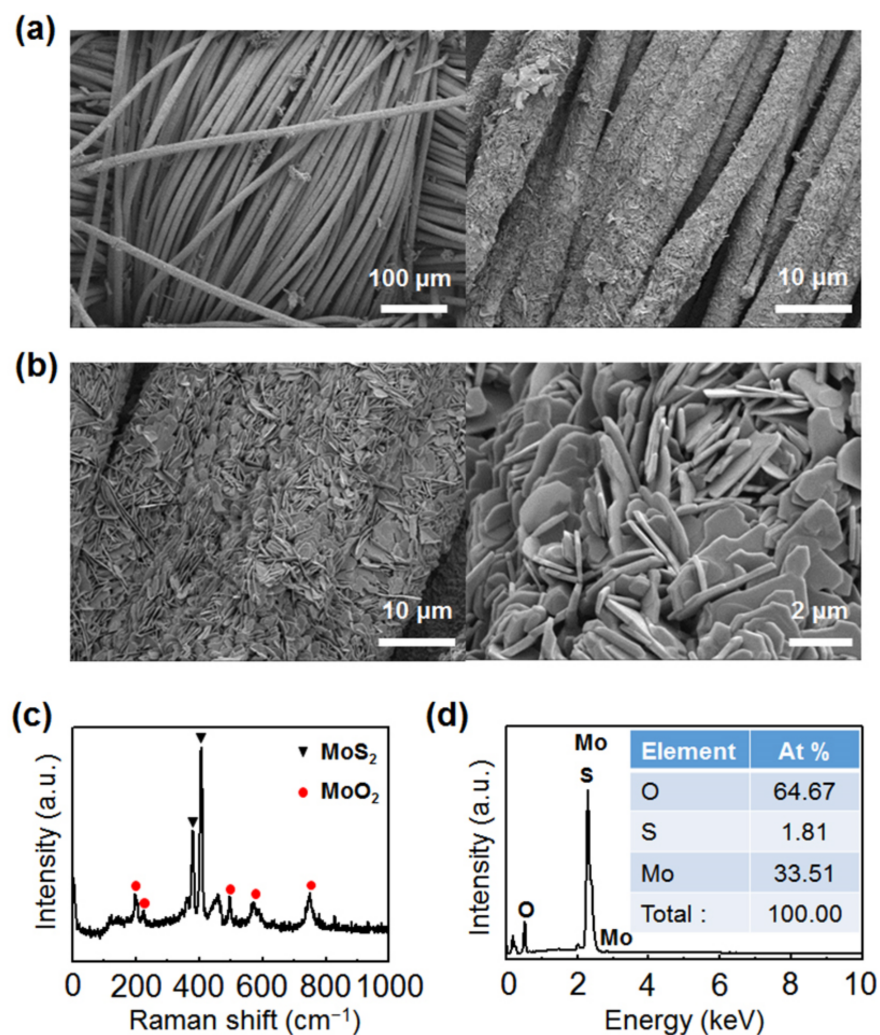


Figure 3. MoO₂-MoS₂ nanoplates grown on carbon cloth after carbon cloth-assisted CVD growth. (a,b) Low-magnification and high-magnification scanning electron microscopy (SEM) images of MoO₂-MoS₂ nanoplates grown on carbon cloth after the carbon cloth-assisted CVD growth. (c) Raman spectrum of MoO₂-MoS₂ nanoplates. (d) SEM-energy-dispersive X-ray spectroscopy (SEM-EDS) data of MoO₂-MoS₂ nanoplates.

Figure 4a is an AFM image of the monolayer MoS₂ synthesized using the carbon cloth-assisted CVD method, which shows that the surface of monolayer MoS₂ was clean without any particles, unlike monolayer MoS₂ synthesized using the conventional CVD method. The line profile obtained along the dotted red line in Figure 4a shows that the thickness of the synthesized monolayer MoS₂ was ~0.988 nm, which is consistent with the reported thickness of monolayer MoS₂ (Figure 4b) [19,46]. Additional AFM data of monolayer MoS₂ are shown in Figure S6. Figure 4c shows an optical image of monolayer MoS₂ grown on an SiO₂/Si substrate. The Raman spectrum (Curve 1) of monolayer MoS₂ taken at point 1 shows the Raman peaks of the E_{12g} mode located at 380 cm⁻¹ and the A_{1g} mode located at 401 cm⁻¹ (Figure 4d) [31]. Curve 2 in Figure 4d shows the Raman spectrum obtained from the substrate at point 2. The PL spectrum (Curve 1) of monolayer MoS₂ shows a strong peak at 1.84 eV (Figure 4e), which is consistent with the A exciton peak due to the direct bandgap of monolayer MoS₂ [19,47]. Curve 2 in Figure 4e is the PL spectrum obtained from the substrate at point 2. Raman and PL maps of MoS₂ show that monolayer MoS₂ exhibited uniform Raman and PL peak intensities, confirming that monolayer MoS₂ had a uniform chemical composition and electronic structure (Figure 4f–h). Figure 4i shows a TEM image of monolayer MoS₂. The high-resolution TEM (HRTEM) image (Figure 4j) and

corresponding selected area electron diffraction (SAED) patterns (Figure 4k) with [001] zone axis confirm the hexagonal lattice structure with the lattice spacing of 0.278 nm assigned to the (100) planes of MoS₂. In addition, TEM–EDS analysis shows that the monolayer MoS₂ consisted of Mo and S, and the ratio of Mo to S elements was 1:2 (Figure 4l). The Cu peak originated from the TEM grid, and the Cr peak came from the pole pieces of the TEM.

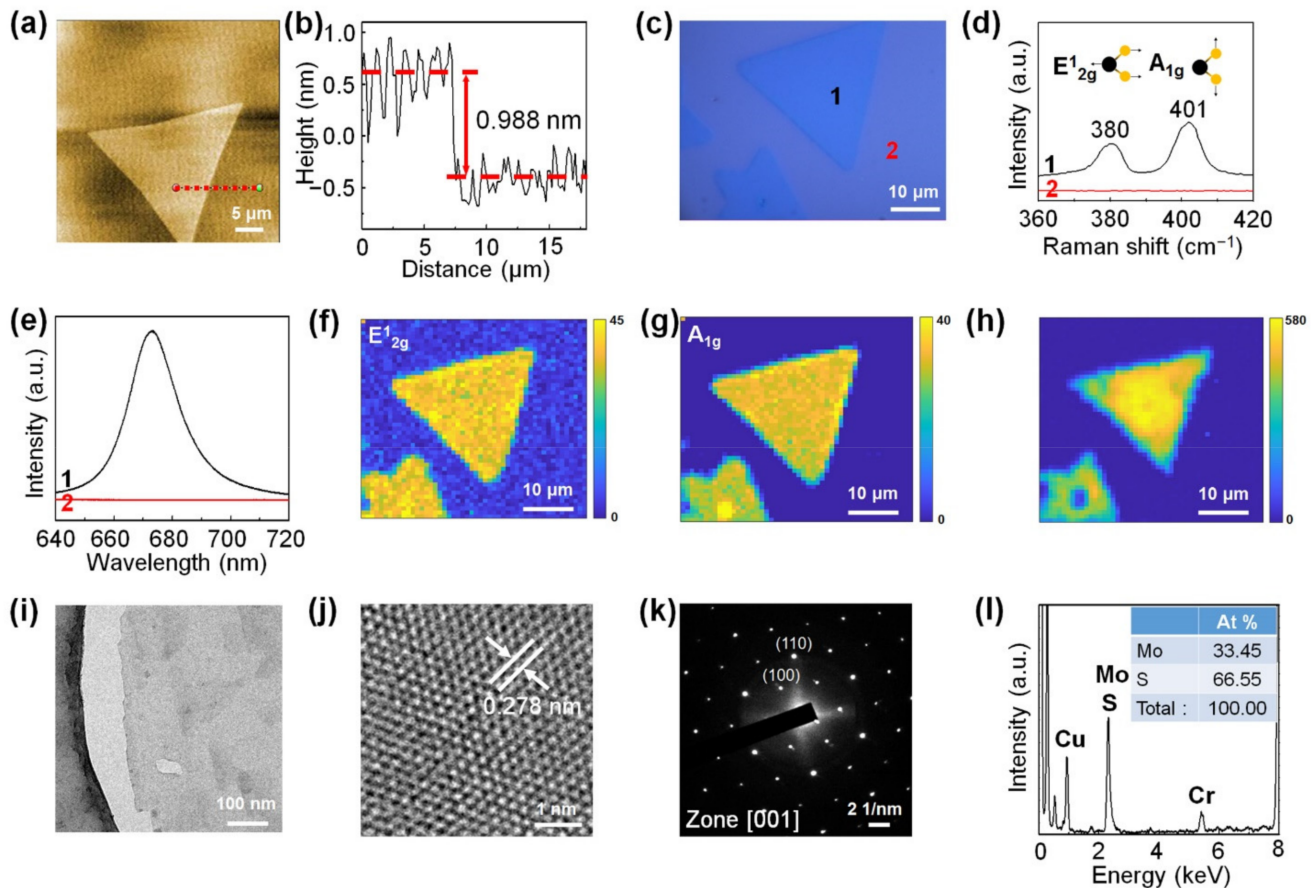


Figure 4. Detailed analysis of monolayer MoS₂ synthesized by CVD growth using carbon cloth. (a) AFM image of monolayer MoS₂. (b) Height line profile along the dotted red line in (a). (c) Optical image of monolayer MoS₂. (d) Raman spectra taken at points 1 and 2 of (c). (e) PL spectra taken at points 1 and 2 of (c). (f,g) Raman maps of the E_{2g} mode and A_{1g} mode of MoS₂, respectively. (h) PL map of monolayer MoS₂. (i) Low-magnification transmission electron microscopy (TEM) image of monolayer MoS₂. (j) High-resolution TEM (HRTEM) image of monolayer MoS₂. (k) Selected area electron diffraction (SAED) patterns of monolayer MoS₂. (l) TEM–energy-dispersive X-ray spectroscopy (TEM–EDS) data of monolayer MoS₂.

Figure 5 shows the growth process of monolayer MoS₂ depending on the reaction time in carbon cloth-assisted CVD growth. The reaction time was set to 5, 15, 20, and 25 min, respectively. Figure 5a–d show the low-magnification and high-magnification optical images of MoS₂ flakes synthesized at each reaction time. At the reaction time of five minutes, small round-shaped MoS₂ seeds were formed (Figure 5a). At the reaction times of 15 and 20 min, triangular monolayer MoS₂ was generated, and its size increased with increasing reaction time (Figure 5b,c). Size distribution of monolayer MoS₂ synthesized at reaction times of 5 min, 15 min, and 20 min is shown in Figure S7. At the reaction time of 25 min, monolayer MoS₂ films were formed (Figure 5d). The growth of monolayer MoS₂ depending on the reaction time can be explained as follows. In the initial stage of the reaction (reaction time: five minutes), S vapor and MoO_{3-x} vapor are supplied on the substrate to form small MoS₂ seeds. As the reaction time increases (reaction time: 15 and 20 min), MoS₂ seeds form on the substrate and grow to form triangular monolayer MoS₂, and as the reaction time increases, the size of the monolayer MoS₂ increases. When the

reaction time is further increased (reaction time: 25 min), S vapor and MoO_{3-x} vapor are continuously supplied to grow triangular monolayer MoS₂ to form monolayer MoS₂ films. Figure 5e shows the Raman spectra of MoS₂ synthesized at each reaction time, confirming that the flakes and films synthesized at all reaction times were composed of MoS₂. Figure 5f shows the PL spectra of MoS₂ formed at each reaction time, confirming that all MoS₂, except for the MoS₂ seeds formed at the reaction time of five minutes, exhibited a strong A exciton peak at 1.84 eV, indicating that the as-synthesized MoS₂ flakes and layers were monolayers. We believe that the variation of the PL peak position originated from the variation of strain or defects of the as-synthesized monolayer MoS₂ [49].

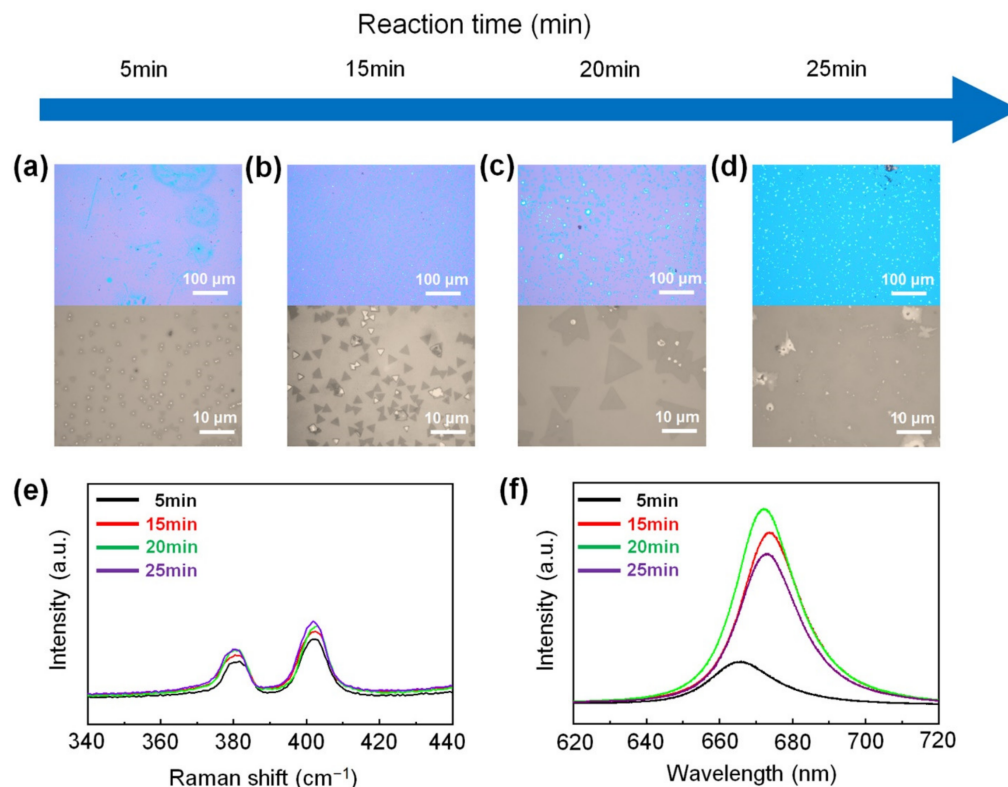


Figure 5. Growth process of monolayer MoS₂ in the carbon cloth-assisted CVD growth. Low-magnification and high-magnification optical images of monolayer MoS₂ synthesized at reaction times of (a) 5 min, (b) 15 min, (c) 20 min, and (d) 25 min, respectively. (e) Raman and (f) PL spectra of monolayer MoS₂ synthesized at reaction times of 5 min, 15 min, 20 min, and 25 min, respectively.

3.3. Monolayer MoS₂ Synthesized Using the Carbon Powder-Assisted CVD Method

The MoS₂ synthesis was conducted using the carbon powder-assisted CVD method to determine whether the large-area growth of monolayer MoS₂ without forming thick MoS₂ films is because carbon acts as a reducing agent or because carbon cloth physically covers the MoO₃ precursor. For carbon powder-assisted CVD synthesis, experiments were conducted by mixing MoO₃ powder and carbon powder in ratios of 1:1, 1:2, 1:3, 1:4, 1:5, and 1:10, respectively.

Figure 6a–f shows low-magnification and high-magnification optical images of monolayer MoS₂ synthesized with various mixing ratios of carbon powder to MoO₃ powder, confirming that monolayer MoS₂ was grown on the substrate over the large area without forming thick films in the center of the substrate. We demonstrated that the carbon material, acting as a reducing agent, plays an important role in the large-area uniform synthesis of monolayer MoS₂. When the mixing ratio of MoO₃ powder to carbon powder was 1:1, the MoS₂ had a nonequilateral triangle shape, which means that MoS₂ has low crystallinity (Figure 6a). This is because when the ratio of carbon powder is low, the degree of the

formation of suboxide MoO_{3-x} species formed during the reaction process is low, so the reaction kinetics deteriorate. When the mixing ratio of the MoO_3 powder to the carbon powder was from 1:2 to 1:10, MoS_2 with an equilateral triangle shape and high crystallinity was formed. Among them, the largest monolayer MoS_2 was obtained when the mixing ratio of MoO_3 powder to carbon powder was 1:5 (Figure 6e). When the mixing ratio of the MoO_3 powder to the carbon powder was further changed to 1:10, the size of the monolayer MoS_2 became small (Figure 6f).

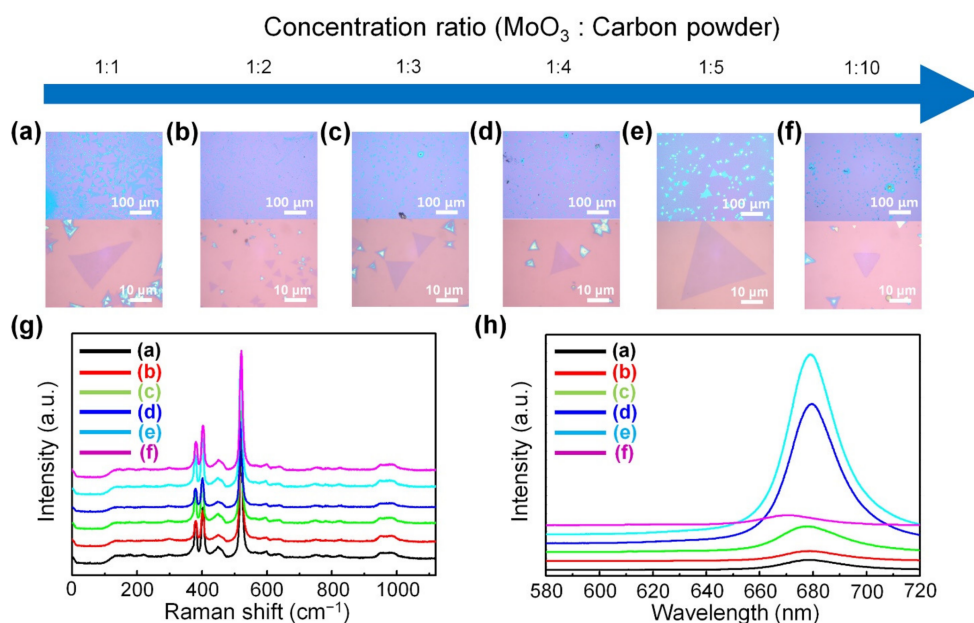


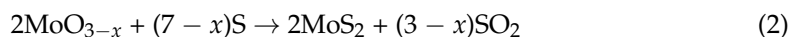
Figure 6. Carbon powder-assisted CVD growth of monolayer MoS_2 . Low-magnification and high-magnification optical images of monolayer MoS_2 synthesized depending on the mixing ratio of carbon powder to MoO_3 powder; (a) 1:1, (b) 1:2, (c) 1:3, (d) 1:4, (e) 1:5, and (f) 1:10, respectively. (g) Raman and (h) PL spectra of monolayer MoS_2 synthesized using the carbon powder-assisted CVD method.

The Raman spectra confirm that all synthesized flakes exhibited Raman peaks at the E_{2g}^1 mode and the A_{1g} mode of MoS_2 (Figure 6g). Figure 6h shows the PL spectra of the MoS_2 synthesized with various mixing ratios of carbon powder to MoO_3 powder. As the ratio of carbon powder increased, monolayer MoS_2 with higher crystallinity was produced, which showed higher PL intensity. The PL spectra of the MoS_2 show strong A exciton peaks at 1.84 eV when the mixing ratio of MoO_3 powder to carbon powder was 1:4 and 1:5, confirming that the as-synthesized MoS_2 flakes were high-quality MoS_2 monolayers. However, when the ratio of carbon powder to MoO_3 powder is too high, MoO_3 is reduced to suboxide MoO_{3-x} species and further reduced to form MoO_2 or Mo, which rather hinders the growth of monolayer MoS_2 . Thus, under this condition, the size of the monolayer MoS_2 became smaller again and the PL intensity decreased.

We performed the synthesis of monolayer MoS_2 using graphite powder mixed with MoO_3 powder (Figure S8). Like the activated carbon powder-assisted CVD method, the graphite powder-assisted CVD method led to the synthesis of monolayer MoS_2 over a large area on the substrate. These results confirm that the reducing property of carbon is the main factor inducing the large-area growth of monolayer MoS_2 .

3.4. Growth Mechanism of Monolayer MoS₂ in the Carbon-Assisted CVD Growth

During the carbon-assisted CVD growth of monolayer MoS₂, MoO₃ is reduced by carbon to form volatile suboxide MoO_{3-x} species, which are further sulfurized to form MoS₂ on an SiO₂/Si substrate. The proposed reaction mechanism is as follows [50,51].



In this paper, we showed that the reaction kinetics for the growth of monolayer MoS₂ can be improved by using carbon materials. When no carbon materials were used, thick MoS₂ films were formed in most areas on the substrate and Figure S1), whereas when carbon materials were used, monolayer MoS₂ was formed in most areas on the substrate (Figure 2, Figure 6 and Figure S3). Thus, we believe that the carbon materials improve the reaction kinetics for the growth of monolayer MoS₂ and suppress the formation of thick MoS₂ films.

The generally accepted mechanism for the growth of monolayer MoS₂ involves the nucleation of tiny suboxide MoO_{3-x} seeds on the substrate surface followed by subsequent sulfurization of these seeds and subsequent growth of monolayer MoS₂ [50]. Thus, suboxide MoO_{3-x} species play a key role in the growth of monolayer MoS₂. By using carbon cloth or carbon powder, we effectively increased the degree of the formation of suboxide MoO_{3-x} species, leading to the growth of monolayer MoS₂ in most areas on the substrate. On the other hand, the formation of thick MoS₂ films can be achieved by either the direct nucleation of nonvolatile MoO₃ or MoO₂ clusters on the substrate followed by subsequent sulfurization.

3.5. Application to Other TMDCs

In addition, to confirm that the carbon cloth-assisted CVD method applies to the synthesis of other monolayer TMDCs, we performed the synthesis of monolayer WS₂ using the conventional CVD method and the carbon cloth-assisted CVD method, respectively. Figure 7a is an optical image of the monolayer WS₂ synthesized using the conventional CVD method. The size of the monolayer WS₂ was as small as four microns, and its shape was not an equilateral triangle. Raman and PL mappings at the 2LA mode and A_{1g} mode of WS₂ show that the monolayer WS₂ exhibited nonuniform Raman and PL peak intensities, confirming that the monolayer WS₂ had nonuniform optical and electronic properties (Figure 7b–d). Figure 7e is an optical image of monolayer WS₂ synthesized using the carbon cloth-assisted CVD method. The size of the monolayer WS₂ was approximately 13.5 microns, and its shape was an equilateral triangle. Raman and PL mappings at the 2LA mode and A_{1g} mode of WS₂ show that the monolayer WS₂ exhibited uniform Raman and PL peak intensities, confirming that monolayer WS₂ had a uniform chemical composition and electronic structure (Figure 7f–h). Figure 7i shows an AFM image of the monolayer WS₂ synthesized using the carbon cloth-assisted CVD method, confirming that the surface of the monolayer WS₂ was clean without any particles. The line profile shows that the thickness of the monolayer WS₂ was ~0.69 nm, which is consistent with the reported thickness of the monolayer WS₂ (Figure 7j) [52,53].

The growth of high-quality monolayer WS₂ by the carbon cloth-assisted CVD method can be explained as follows. For the synthesis of monolayer WS₂, WO₃ powder was used as a precursor. The WO₃ has a significantly high melting point (1473 °C) and its vapor pressure is very low at the reaction temperature (950 °C). Thus, the conventional CVD method produces small monolayer flakes of WS₂ with very low coverage on the substrate (Figure S9). When carbon cloth is placed on top of WO₃ powder, carbon acts as a reducing agent and increases the degree of the formation of suboxide WO_{3-x} species to improve the reaction kinetics for the formation of monolayer WS₂. Thus, under this condition, triangular monolayer WS₂ with increased size forms uniformly on the substrate

(Figure S9). Consequently, we confirmed that the carbon cloth-assisted CVD method is generally applicable to the synthesis of high-quality monolayer WS₂.

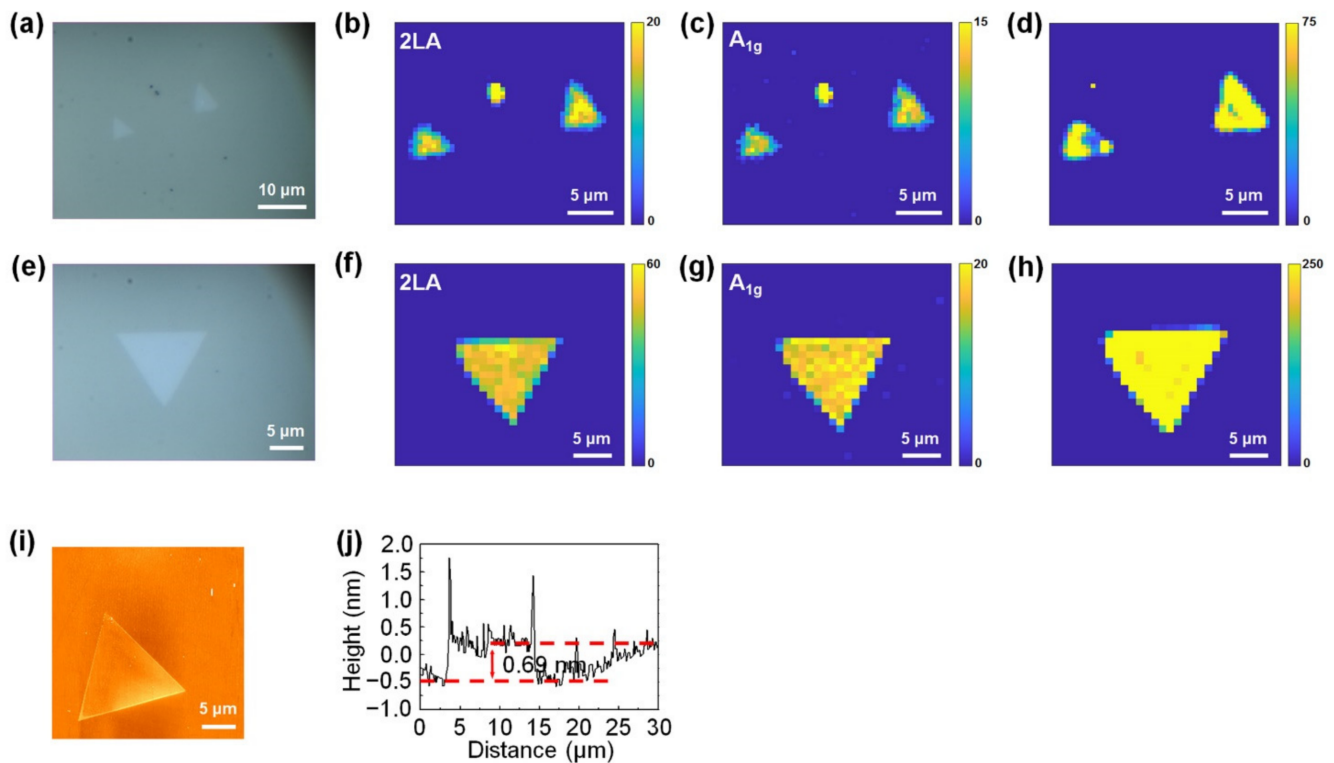


Figure 7. Conventional CVD growth and carbon cloth-assisted CVD growth of monolayer WS₂. (a) Optical image of monolayer WS₂ synthesized using the conventional CVD method. (b,c) Raman maps of monolayer WS₂ synthesized using the conventional CVD method, taken at the 2LA mode and the A_{1g} mode of WS₂, respectively. (d) PL map of monolayer WS₂ synthesized using the conventional CVD method. (e) Optical image of monolayer WS₂ synthesized using the carbon cloth-assisted CVD method. (f,g) Raman maps of monolayer WS₂ synthesized using the carbon cloth-assisted CVD method, taken at the 2LA mode and A_{1g} mode of WS₂, respectively. (h) PL map of monolayer WS₂ synthesized using the carbon cloth-assisted method. (i,j) AFM image and height line profiles of monolayer WS₂ synthesized using carbon cloth-assisted CVD method.

4. Conclusions

We developed a novel carbon-assisted CVD method for large-area uniform growth of high-quality monolayer MoS₂. Using the carbon cloth-assisted CVD method, we synthesized high-quality monolayer MoS₂ uniformly over a large area on the substrate without forming thick MoS₂ films. Through detailed analyses of the carbon cloth that was used in the reaction and experiments with varying reaction times, we revealed the mechanisms for the large-area growth of high-quality monolayer MoS₂. In addition, we showed that the carbon powder-assisted CVD method also produces high-quality monolayer MoS₂ over a large area on the substrate. This confirms that the uniform large-area growth of MoS₂ using the carbon cloth-assisted CVD method is mainly due to the reducing properties of the carbon material. Furthermore, we demonstrated that the carbon cloth-assisted CVD method can be generally used to synthesize monolayer WS₂.

Supplementary Materials: The following are available online at <https://www.mdpi.com/article/10.3390/nano11092423/s1>, Figure S1: Additional optical characterization of the MoS₂ grown using the conventional CVD method, Figure S2: MoS₂ synthesized by the CVD method using H₂ as a carrier gas with Ar, Figure S3: Additional optical characterization of the MoS₂ grown using the carbon cloth-assisted CVD method, Figure S4: MoS₂ flakes grown using the carbon cloth-assisted

CVD growth, Figure S5: MoO₂-MoS₂ nanoplates grown after the carbon cloth-assisted CVD growth and after the conventional CVD growth, Figure S6: Additional AFM data of monolayer MoS₂ synthesized using the carbon cloth-assisted CVD method, Figure S7: Size distribution of monolayer MoS₂ synthesized at reaction times of 5 min, 15 min, and 20 min using the carbon cloth-assisted CVD method, respectively, Figure S8: Graphite powder-assisted CVD growth of monolayer MoS₂, Figure S9: Monolayer WS₂ synthesized on a c-cut sapphire substrate using the conventional CVD method and the carbon cloth-assisted CVD method.

Author Contributions: Conceptualization, Y.Y.; investigation, J.B. and Y.Y.; writing—original draft preparation, J.B. and Y.Y.; writing—review and editing, Y.Y.; supervision, Y.Y.; funding acquisition, Y.Y. All authors have read and agreed to the published version of the manuscript.

Funding: This work was supported by the National Research Foundation of Korea (NRF) grant funded by the Korea government (MSIT) (2019R1C1C1008070 and 2018R1C1B5044670). This work was supported by Institute of Information & communications Technology Planning & Evaluation (IITP) grant funded by the Korea government (MSIT) (2021-0-00185). This research was supported by Basic Science Research Program through the National Research Foundation of Korea (NRF) funded by the Ministry of Education (2021R1A6A1A10044950). This research was supported by Nano-Material Technology Development Program through the NRF funded by the MSIT (2009-0082580).

Conflicts of Interest: The authors declare no conflict of interest.

References

1. Geim, A.K.; Novoselov, K.S. The rise of graphene. *Nat. Mater.* **2007**, *6*, 183–191. [[CrossRef](#)]
2. Neto, A.C.; Guinea, F.; Peres, N.M.; Novoselov, K.S.; Geim, A.K. The electronic properties of graphene. *Rev. Mod. Phys.* **2009**, *81*, 109. [[CrossRef](#)]
3. Wilson, J.A.; Yoffe, A. The transition metal dichalcogenides discussion and interpretation of the observed optical, electrical and structural properties. *Adv. Phys.* **1969**, *18*, 193–335. [[CrossRef](#)]
4. Wang, Q.H.; Kalantar-Zadeh, K.; Kis, A.; Coleman, J.N.; Strano, M.S. Electronics and optoelectronics of two-dimensional transition metal dichalcogenides. *Nat. Nanotechnol.* **2012**, *7*, 699–712. [[CrossRef](#)] [[PubMed](#)]
5. Manzeli, S.; Ovchinnikov, D.; Pasquier, D.; Yazyev, O.V.; Kis, A. 2D transition metal dichalcogenides. *Nat. Rev. Mater.* **2017**, *2*, 1–15. [[CrossRef](#)]
6. Allen, M.J.; Tung, V.C.; Kaner, R.B. Honeycomb carbon: A review of graphene. *Chem. Rev.* **2010**, *110*, 132–145. [[CrossRef](#)]
7. Mak, K.F.; Shan, J. Photonics and optoelectronics of 2D semiconductor transition metal dichalcogenides. *Nat. Photonics* **2016**, *10*, 216–226. [[CrossRef](#)]
8. Radisavljevic, B.; Radenovic, A.; Brivio, J.; Giacometti, V.; Kis, A. Single-layer MoS₂ transistors. *Nat. Nanotechnol.* **2011**, *6*, 147–150. [[CrossRef](#)]
9. Li, H.; Yin, Z.; He, Q.; Li, H.; Huang, X.; Lu, G.; Fam, D.W.H.; Tok, A.I.Y.; Zhang, Q.; Zhang, H. Fabrication of single-and multilayer MoS₂ film-based field-effect transistors for sensing NO at room temperature. *Small* **2012**, *8*, 63–67. [[CrossRef](#)]
10. Vaknin, Y.; Dagan, R.; Rosenwaks, Y. Schottky Barrier Height and Image Force Lowering in Monolayer MoS₂ Field Effect Transistors. *Nanomaterials* **2020**, *10*, 2346. [[CrossRef](#)]
11. Lopez-Sanchez, O.; Lembke, D.; Kayci, M.; Radenovic, A.; Kis, A. Ultrasensitive photodetectors based on monolayer MoS₂. *Nat. Nanotechnol.* **2013**, *8*, 497–501. [[CrossRef](#)] [[PubMed](#)]
12. Kim, S.; Park, W.; Kim, D.; Kang, J.; Lee, J.; Jang, H.Y.; Song, S.H.; Cho, B.; Lee, D. Novel Exfoliation of High-Quality 2H-MoS₂ Nanoflakes for Solution-Processed Photodetector. *Nanomaterials* **2020**, *10*, 1045. [[CrossRef](#)]
13. Li, H.; Tsai, C.; Koh, A.L.; Cai, L.; Contryman, A.W.; Fragapane, A.H.; Zhao, J.; Han, H.S.; Manoharan, H.C.; Abild-Pedersen, F.; et al. Activating and optimizing MoS₂ basal planes for hydrogen evolution through the formation of strained sulphur vacancies. *Nat. Mater.* **2016**, *15*, 48–53. [[CrossRef](#)] [[PubMed](#)]
14. Huang, P.C.; Wu, C.L.; Brahma, S.; Shaikh, M.O.; Huang, J.L.; Lee, J.J.; Wang, S.C. MoS₂-Carbon Inter-overlapped Structures as Effective Electrocatalysts for the Hydrogen Evolution Reaction. *Nanomaterials* **2020**, *10*, 1389. [[CrossRef](#)] [[PubMed](#)]
15. Zhang, J.; Wu, J.; Guo, H.; Chen, W.; Yuan, J.; Martinez, U.; Gupta, G.; Mohite, A.; Ajayan, P.M.; Lou, J. Unveiling active sites for the hydrogen evolution reaction on monolayer MoS₂. *Adv. Mater.* **2017**, *29*, 1701955. [[CrossRef](#)] [[PubMed](#)]
16. Mak, K.F.; Lee, C.; Hone, J.; Shan, J.; Heinz, T.F. Atomically thin MoS₂: A new direct-gap semiconductor. *Phys. Rev. Lett.* **2010**, *105*, 136805. [[CrossRef](#)]
17. Steinhoff, A.; Kim, J.H.; Jahnke, F.; Rosner, M.; Kim, D.S.; Lee, C.; Han, G.H.; Jeong, M.S.; Wehling, T.O.; Gies, C. Efficient Excitonic Photoluminescence in Direct and Indirect Band Gap Monolayer MoS₂. *Nano Lett.* **2015**, *15*, 6841–6847. [[CrossRef](#)]
18. Niu, Y.; Gonzalez-Abad, S.; Frisenda, R.; Marauhn, P.; Drüppel, M.; Gant, P.; Schmidt, R.; Taghavi, N.S.; Barcons, D.; Molina-Mendoza, A.J.; et al. Thickness-Dependent Differential Reflectance Spectra of Monolayer and Few-Layer MoS₂, MoSe₂, WS₂ and WSe₂. *Nanomaterials* **2018**, *8*, 725. [[CrossRef](#)]

19. Splendiani, A.; Sun, L.; Zhang, Y.; Li, T.; Kim, J.; Chim, C.Y.; Galli, G.; Wang, F. Emerging photoluminescence in monolayer MoS₂. *Nano Lett.* **2010**, *10*, 1271–1275. [[CrossRef](#)]
20. Liu, X.; Galfsky, T.; Sun, Z.; Xia, F.; Lin, E.-c.; Lee, Y.-H.; Kéna-Cohen, S.; Menon, V.M. Strong light–matter coupling in two-dimensional atomic crystals. *Nat. Photonics* **2015**, *9*, 30–34. [[CrossRef](#)]
21. Yin, Z.; Li, H.; Li, H.; Jiang, L.; Shi, Y.; Sun, Y.; Lu, G.; Zhang, Q.; Chen, X.; Zhang, H. Single-layer MoS₂ phototransistors. *ACS Nano* **2012**, *6*, 74–80. [[CrossRef](#)] [[PubMed](#)]
22. Zhang, W.; Huang, J.K.; Chen, C.H.; Chang, Y.H.; Cheng, Y.J.; Li, L.J. High-gain phototransistors based on a CVD MoS₂ monolayer. *Adv. Mater.* **2013**, *25*, 3456–3461. [[CrossRef](#)] [[PubMed](#)]
23. Li, H.; Wu, J.; Yin, Z.; Zhang, H. Preparation and applications of mechanically exfoliated single-layer and multilayer MoS₂ and WSe₂ nanosheets. *Acc. Chem. Res.* **2014**, *47*, 1067–1075. [[CrossRef](#)] [[PubMed](#)]
24. Yi, M.; Shen, Z. A review on mechanical exfoliation for the scalable production of graphene. *J. Mater. Chem. A* **2015**, *3*, 11700–11715. [[CrossRef](#)]
25. Zeng, Z.; Yin, Z.; Huang, X.; Li, H.; He, Q.; Lu, G.; Boey, F.; Zhang, H. Single-layer semiconducting nanosheets: High-yield preparation and device fabrication. *Angew. Chem.* **2011**, *50*, 11093–11097. [[CrossRef](#)]
26. Dumcenco, D.; Ovchinnikov, D.; Marinov, K.; Lazic, P.; Gibertini, M.; Marzari, N.; Lopez Sanchez, O.; Kung, Y.C.; Krasnozhan, D.; Chen, M.W.; et al. Large-Area Epitaxial Monolayer MoS₂. *ACS Nano* **2015**, *9*, 4611–4620. [[CrossRef](#)]
27. Cai, Z.; Liu, B.; Zou, X.; Cheng, H.-M. Chemical vapor deposition growth and applications of two-dimensional materials and their heterostructures. *Chem. Rev.* **2018**, *118*, 6091–6133. [[CrossRef](#)]
28. Wang, X.; Feng, H.; Wu, Y.; Jiao, L. Controlled synthesis of highly crystalline MoS₂ flakes by chemical vapor deposition. *J. Am. Chem. Soc.* **2013**, *135*, 5304–5307. [[CrossRef](#)]
29. Lee, Y.H.; Zhang, X.Q.; Zhang, W.; Chang, M.T.; Lin, C.T.; Chang, K.D.; Yu, Y.C.; Wang, J.T.; Chang, C.S.; Li, L.J.; et al. Synthesis of large-area MoS₂ atomic layers with chemical vapor deposition. *Adv. Mater.* **2012**, *24*, 2320–2325. [[CrossRef](#)]
30. Wang, S.; Rong, Y.; Fan, Y.; Pacios, M.; Bhaskaran, H.; He, K.; Warner, J.H. Shape evolution of monolayer MoS₂ crystals grown by chemical vapor deposition. *Chem. Mater.* **2014**, *26*, 6371–6379. [[CrossRef](#)]
31. Ling, X.; Lee, Y.H.; Lin, Y.; Fang, W.; Yu, L.; Dresselhaus, M.S.; Kong, J. Role of the seeding promoter in MoS₂ growth by chemical vapor deposition. *Nano Lett.* **2014**, *14*, 464–472. [[CrossRef](#)] [[PubMed](#)]
32. Özden, A.; Ay, F.; Sevik, C.; Perkgöz, N.K. CVD growth of monolayer MoS₂: Role of growth zone configuration and precursors ratio. *Jpn. J. Appl. Phys.* **2017**, *56*, 06GG05. [[CrossRef](#)]
33. Chowdhury, S.; Roy, A.; Liu, C.; Alam, M.H.; Ghosh, R.; Chou, H.; Akinwande, D.; Banerjee, S.K. Two-Step Growth of Uniform Monolayer MoS₂ Nanosheets by Metal–Organic Chemical Vapor Deposition. *ACS Omega* **2021**, *6*, 10343–10351. [[CrossRef](#)]
34. Lin, Z.; Zhao, Y.; Zhou, C.; Zhong, R.; Wang, X.; Tsang, Y.H.; Chai, Y. Controllable Growth of Large–Size Crystalline MoS₂ and Resist-Free Transfer Assisted with a Cu Thin Film. *Sci. Rep.* **2015**, *5*, 18596. [[CrossRef](#)]
35. Ji, Q.; Zhang, Y.; Zhang, Y.; Liu, Z. Chemical vapour deposition of group-VIB metal dichalcogenide monolayers: Engineered substrates from amorphous to single crystalline. *Chem. Soc. Rev.* **2015**, *44*, 2587–2602. [[CrossRef](#)]
36. Zhou, D.; Shu, H.; Hu, C.; Jiang, L.; Liang, P.; Chen, X. Unveiling the Growth Mechanism of MoS₂ with Chemical Vapor Deposition: From Two-Dimensional Planar Nucleation to Self-Seeding Nucleation. *Cryst. Growth Des.* **2018**, *18*, 1012–1019. [[CrossRef](#)]
37. Senthilkumar, V.; Tam, L.C.; Kim, Y.S.; Sim, Y.; Seong, M.-J.; Jang, J.I. Direct vapor phase growth process and robust photoluminescence properties of large area MoS₂ layers. *Nano Res.* **2014**, *7*, 1759–1768. [[CrossRef](#)]
38. Zhang, X.; Nan, H.; Xiao, S.; Wan, X.; Ni, Z.; Gu, X.; Ostrikov, K. Shape-Uniform, High-Quality Monolayered MoS₂ Crystals for Gate-Tunable Photoluminescence. *ACS Appl. Mater. Interfaces* **2017**, *9*, 42121–42130. [[CrossRef](#)]
39. Zhang, X.; Nan, H.; Xiao, S.; Wan, X.; Gu, X.; Du, A.; Ni, Z.; Ostrikov, K. Transition metal dichalcogenides bilayer single crystals by reverse-flow chemical vapor epitaxy. *Nat. Commun.* **2019**, *10*, 598. [[CrossRef](#)] [[PubMed](#)]
40. Ahn, C.; Park, Y.; Shin, S.; Ahn, J.-G.; Song, I.; An, Y.; Jung, J.; Kim, C.S.; Kim, J.H.; Bang, J.; et al. Growth of Monolayer and Multilayer MoS₂ Films by Selection of Growth Mode: Two Pathways via Chemisorption and Physisorption of an Inorganic Molecular Precursor. *ACS Appl. Mater. Interfaces* **2021**, *13*, 6805–6812. [[CrossRef](#)] [[PubMed](#)]
41. Kang, K.; Xie, S.; Huang, L.; Han, Y.; Huang, P.Y.; Mak, K.F.; Kim, C.-J.; Muller, D.; Park, J. High-mobility three-atom-thick semiconducting films with wafer-scale homogeneity. *Nature* **2015**, *520*, 656–660. [[CrossRef](#)]
42. Cheng, Z.; Xia, M.; Hu, R.; Liang, C.; Liang, G.; Zhang, S. Single crystal monolayer MoS₂ triangles with wafer-scale spatial uniformity by MoO₃ pre-deposited chemical vapor deposition. *J. Cryst. Growth* **2017**, *480*, 6–12. [[CrossRef](#)]
43. Yu, H.; Liao, M.; Zhao, W.; Liu, G.; Zhou, X.J.; Wei, Z.; Xu, X.; Liu, K.; Hu, Z.; Deng, K.; et al. Wafer-Scale Growth and Transfer of Highly-Oriented Monolayer MoS₂ Continuous Films. *ACS Nano* **2017**, *11*, 12001–12007. [[CrossRef](#)] [[PubMed](#)]
44. Yang, P.; Zou, X.; Zhang, Z.; Hong, M.; Shi, J.; Chen, S.; Shu, J.; Zhao, L.; Jiang, S.; Zhou, X.; et al. Batch production of 6-inch uniform monolayer molybdenum disulfide catalyzed by sodium in glass. *Nat. Commun.* **2018**, *9*, 979. [[CrossRef](#)] [[PubMed](#)]
45. Wang, P.; Lei, J.; Qu, J.; Cao, S.; Jiang, H.; He, M.; Shi, H.; Sun, X.; Gao, B.; Liu, W. Mechanism of Alkali Metal Compound-Promoted Growth of Monolayer MoS₂: Eutectic Intermediates. *Chem. Mater.* **2019**, *31*, 873–880. [[CrossRef](#)]
46. Yang, X.; Li, B. Monolayer MoS₂ for nanoscale photonics. *Nanophotonics* **2020**, *9*, 1557–1577. [[CrossRef](#)]
47. Feng, S.; Tan, J.; Zhao, S.; Zhang, S.; Khan, U.; Tang, L.; Zou, X.; Lin, J.; Cheng, H.M.; Liu, B. Synthesis of Ultrahigh-Quality Monolayer Molybdenum Disulfide through In Situ Defect Healing with Thiol Molecules. *Small* **2020**, *16*, 2003357. [[CrossRef](#)]

48. DeGregorio, Z.P.; Yoo, Y.; Johns, J.E. Aligned MoO₂/MoS₂ and MoO₂/MoTe₂ Freestanding Core/Shell Nanoplates Driven by Surface Interactions. *J. Phys. Chem. Lett.* **2017**, *8*, 1631–1636. [[CrossRef](#)]
49. Conley, H.J.; Wang, B.; Ziegler, J.I.; Haglund, R.F.; Pantelides, S.T.; Bolotin, K.I. Bandgap Engineering of Strained Monolayer and Bilayer MoS₂. *Nano Lett.* **2013**, *13*, 3626–3630. [[CrossRef](#)]
50. Cain, J.D.; Shi, F.; Wu, J.; Dravid, V.P. Growth Mechanism of Transition Metal Dichalcogenide Monolayers: The Role of Self-Seeding Fullerene Nuclei. *ACS Nano* **2016**, *10*, 5440–5445. [[CrossRef](#)]
51. Choi, S.H.; Stephen, B.; Park, J.-H.; Lee, J.S.; Kim, S.M.; Yang, W.; Kim, K.K. Water-Assisted Synthesis of Molybdenum Disulfide Film with Single Organic Liquid Precursor. *Sci. Rep.* **2017**, *7*, 1983. [[CrossRef](#)] [[PubMed](#)]
52. Gutiérrez, H.R.; Perea-López, N.; Elías, A.L.; Berkdemir, A.; Wang, B.; Lv, R.; López-Urías, F.; Crespi, V.H.; Terrones, H.; Terrones, M. Extraordinary room-temperature photoluminescence in triangular WS₂ monolayers. *Nano Lett.* **2013**, *13*, 3447–3454. [[CrossRef](#)] [[PubMed](#)]
53. Cong, C.; Shang, J.; Wu, X.; Cao, B.; Peimyoo, N.; Qiu, C.; Sun, L.; Yu, T. Synthesis and optical properties of large-area single-crystalline 2D semiconductor WS₂ monolayer from chemical vapor deposition. *Adv. Opt. Mater.* **2014**, *2*, 131–136. [[CrossRef](#)]